Experimental Determination and Validation of sUAS Moments of Inertia

Presented in Partial Fulfillment of the Requirements for Undergraduate Honors Research Distinction in the Undergraduate School of The Ohio State University

By

Michael Kevin Thomas

The Ohio State University

Department of Mechanical and Aerospace Engineering

May 2020

Defense Committee

Dr. James Gregory, Advisor

Dr. Matthew McCrink, Co-advisor

Abstract

The rise in use of small unmanned aerial systems (sUAS) in industry and research has resulted in a need to develop modeling and testing procedures which are feasible and cost effective for small-scale airframes. Computer models of these vehicles are based on a description of the underlying physical and aerodynamic characteristics of these vehicles which are often only roughly approximated in the design stage. One difficult to accurately obtain, yet highly important, physical characteristic of an aircraft is its inertia tensor. The aircraft's inertia tensor is directly related to the dynamic motion about the pitch, roll, and yaw axes. Understanding this dynamic motion is the first step in control system design and validation. Utilizing previous work in experimental moment of inertia (MOI) testing and small-scale flight testing, this project developed a bifilar torsional pendulum capable of accurately and affordably measuring the inertia tensor of sUAS. In order to validate the bifilar pendulum measurements, flight tests were developed to experimentally obtain the MOI of the sUAS for comparison. Due to changes in Ohio State University policy after the outbreak of COVID-19, the planned flight tests could not be completed at this time. Future work should focus on the validation of the bifilar pendulum measurements along with determination and validation of MOI for non-primary axes.

Acknowledgements

I would like to sincerely thank my advisors, Dr. James Gregory and Dr. Matthew McCrink, for providing the opportunity to conduct my own research as an undergraduate student. With their encouragement and guidance, I have been able to accomplish more than I could have imagined. It has been a pleasure to work in their lab over the past two years, and I am thankful to have them both as mentors.

I was also fortunate to have the support and guidance of graduate and undergraduate students in the lab throughout my project. First, I would like to thank Ross Heidersbach for his previous work with the bifilar pendulum, and his help and guidance on the reconstruction of the Mentor-G V1. I would also like to thank Shane Vitullo for his help during ground testing and engine testing of the Mentor-G V1. Many others in my lab have helped me along the way, providing assistance with testing and helping to diagnose problems. I would like to thank all of them for their support.

Finally, I would like to thank my friends, family, and my girlfriend for supporting and encouraging me throughout my undergraduate career. I would not be here without them, and I am thankful for their continued support.

Table of Contents

List of Tables

List of Figures

List of Variables

α = angle of attack
C = damping Coefficient
$\overline{C}$ = mean chord
C_D = coefficient of drag
$C_{D\alpha}$ = variation of coefficient of drag with change in angle of attack
C_L = coefficient of lift
$C_{L\alpha}$ = variation of coefficient of lift with change in angle of attack
$C_{m\alpha}$ = variation of moment coefficient with change in attack
C_{mq} = variation of moment coefficient with change in velocity
D = displacement between vertical pendulum wires
g = gravitational acceleration
h = length of pendulum wires
I = moment of Inertia
K_D = damping Coefficient
m = mass
P_o = stagnation pressure
P_s = static pressure
ρ = air density
ρ_{SL} = standard sea level air density
S = wing area
V = velocity
$\overline{V}$ = steady state velocity
Θ = displacement Angle

Chapter 1: Introduction

1.1 Overview

The first chapter discusses the recreation of a previously developed method for measuring the moment of inertia (MOI) of small unmanned aerial systems (sUAS). The method utilizes a bifilar torsional pendulum in conjunction with a MATLAB program to compare computational pendulum dynamics with the experimental dynamics and estimate the pendulum's MOI. Additionally, the determination and mitigation of pendulum errors was also examined. Finally, the accuracy of the pendulum was assessed through the use of simply shaped test objects.

The second chapter discusses the development and completion of flight tests which were used to validate the MOI values measured by the bifilar pendulum.

1.2 Motivation

Flight testing has been a part of aerospace engineering since the dawn of aviation. One of the most important aspects of flight testing is the testing of the aircraft's stability along its three main axes (longitudinal, lateral, and directional) as well as the cross-coupling that can occur between these axes. If unchecked, this cross coupling can lead to dramatic and unexpected departures from controlled flight. Before this testing can occur, dynamic models are developed early in the design cycle which approximate how the aircraft will behave in flight. The accuracy of the model is highly dependent on the measured or calculated airframe parameters used in the model. One of the most impactful parameters is the inertia tensor; however, it is traditionally a difficult parameter to obtain, especially for sUAS.[1] With the increase in use of sUAS for both research

and commercial applications, this has become an important field of study. Developing accurate methods of determining the inertia tensor for sUAS as well as new methods of flight testing to confirm the accuracy of the aircraft model is a crucial step in safely integrating sUAS into the National Airspace System (NAS). It is within this context that we are partnering with the FAA through the ASSURE Center of Excellence to develop not only algorithms and techniques for certifying sUAS, but also influencing the policy underlying the adoption of sUAS for widespread use in the NAS.

The importance of obtaining an accurate inertia tensor for a given airframe has been a driving force for the research of simple and cost effective methods, but most of this research has been focused on full-scale manned aircraft.[1,2,3] Because of this focus, many of these methods are infeasible for use in sUAS applications. For example, NASA's Dynamic Inertia Method requires the use of large-scale test stands as well as high-tech sensors and equipment which would overshadow the cost of sUAS by hundreds of thousands of dollars.[1] This creates the need for a low-cost option feasible for sUAS application. Most of the difficulties with characterizing sUAS airframes deal with the small size of the aircraft compared to typical general aviation aircraft as well as the possible inaccuracies in their construction. Computer-aided design (CAD) models can provide accurate MOI measurements; however, the typical workshop style construction of sUAS can cause significant differences between the designed model and the physical aircraft due to poor quality control, imperfect materials, and vehicle repairs/modifications. This highlights the need for accurate experimental methods that are applicable to small-scale aircraft.

Aircraft flight testing has continued to incorporate new technologies and methods throughout history in order to understand the capabilities of newly developed aircraft, but these methods

have again focused on full-scale manned aircraft.[4,5] The rise of sUAS creates the need to adapt these flight testing methods in order to better meet the challenges and requirements of sUAS. Regarding flying qualities, they are inherently more susceptible to turbulence and have higher longitudinal, directional, and lateral control sensitivities. Regarding data acquisition, the small airframes and low weight requirements ultimately limit the number of variables that can be monitored due to the size and weight of additional sensors.

This research project will build upon previous work in order to fully develop an accurate and low-cost solution for characterizing the dynamic motion of sUAS airframes. Understanding this dynamic motion is critical for assessing vehicle models and their associated control systems. sUAS offer a wide variety of applications; however, the ability to accurately model and assess the performance of these vehicles is a vital step in reaching the full potential of sUAS technology.

1.3 Bifilar Torsional Pendulum Background

Jardin and Mueller developed an experimental moment of inertia testing procedure utilizing a nonlinear bifilar pendulum model.[6] “A bifilar (two-wire) pendulum is a torsional pendulum consisting of a test object suspended by two thin parallel wires. The pendulum oscillates about the vertical axis. The restoring torque of the bifilar pendulum is provided by the gravitational force as rotations from the rest state cause the test object to raise slightly.”. [6] Figure 1.1 shows a representation of the system, and the nonlinear equation of motion is shown in equation 1.1.

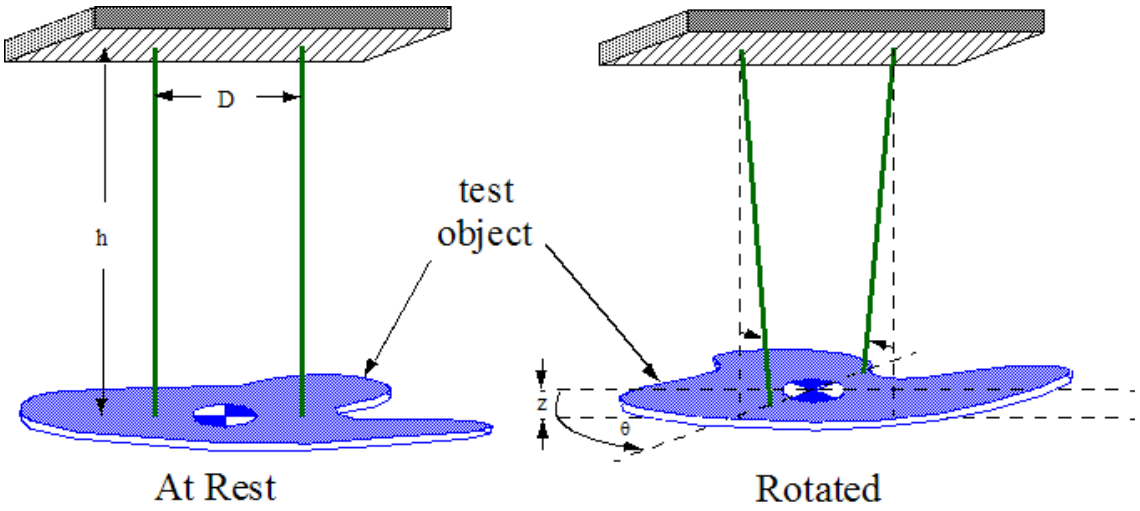

Figure 1.1: Bifilar Pendulum Model [6]

$$\ddot{\theta} + \left(\frac{K_D}{I}\,\dot{\theta}|\dot{\theta}| + \frac{C}{I}\dot{\theta}\right) + \left(\frac{mgD^2}{4Ih}\right)\frac{\sin\theta}{\sqrt{1 - 0.5\left(\frac{D}{h}\right)^2(1-\cos\theta)}} = 0 \qquad [1.1]$$

Starting from the left side of equation 1.1, the first term is the angular acceleration of the bifilar pendulum. The second group of terms is related to the damping of the pendulum oscillation. K_D is a lumped coefficient regarding the air resistance on the pendulum, and C is the lumped coefficient of the general damping resistance from energy losses in the system. Both of the damping terms are divided by the moment of inertia (I) and multiplied by the angular velocity. The last set of terms contains the bifilar pendulum parameters such as the pendulum's mass (m), displacement between the vertical strings (D), and the vertical distance of the string (h). The last set of terms also contains the gravitational acceleration constant (g), and the angular displacement (Θ).

Jardin and Mueller's method used the bifilar torsional pendulum to obtain rotational data (with a small inertial navigation system to record the data) and a parameter estimation technique in Simulink in order to determine the moments of inertia about the principle axes of a fixed-wing sUAS. Within the Simulink model, an Ode45 function programmed with equation 1.1 was used to simulate the bifilar pendulum motion with an optimization function providing the changing MOI and damping coefficients. The optimization function then finds the minimum error between the simulated results and the experimental data in order to determine the system's MOI and damping coefficients.

Due to the research's focus on measuring the MOI about the z-axis of the aircraft (which has the lowest drag effect due to the aircraft's geometry), there was limited work done to characterize the drag effects which will be more prominent in the MOI measurements about the y and x axes. The orientation of the primary aircraft axes (x, y, and z) is shown in figure 1.2.

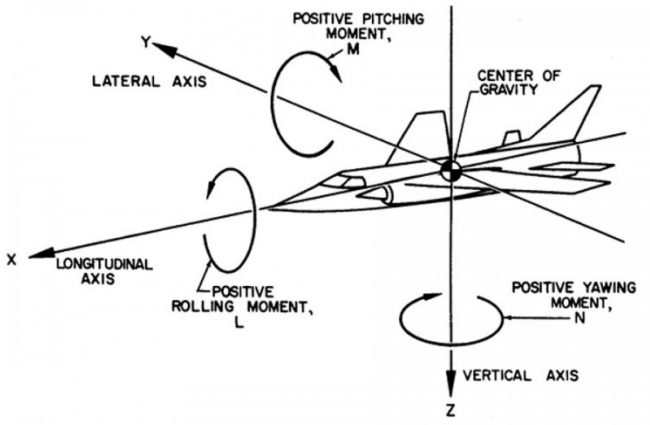

Figure 1.2: Representation of Aircraft Axes [11]

1.4 Flight Test Background

Flight testing is typically one of the last steps in the development or remodeling of an aircraft and serves the purpose of an experimental validation on the prior calculations and computational results. The flight testing in this project will serve the same purpose of providing an experimental validation for the moment of inertia results from the bifilar pendulum testing.

Landman discussed the benefits of testing the physical aircraft instead of computer or wind tunnel models.[7] Some aircraft parameters (such as control effectiveness and MOI) can be very sensitive to small differences between the aircraft and model(s) which often occur in sUAS. This previous research shows the benefit of experimental validation of MOI through dynamic flight testing.

Before the moment of inertia flight tests can be performed, the sUAS must undergo an airspeed calibration test in order to calibrate the airspeed readings from the sUAS's pitot static probe. The sUAS's pitot static probe measures both the total freestream pressure and the static freestream pressure and uses the difference in these pressures to determine the indicated airspeed (IAS) from equation 1.2.

$$IAS = \sqrt{\frac{2\times(P_o - P_s)}{\rho_{SL}}} \qquad [1.2]$$

Due to the pitot static probe being attached to the aircraft, the flow dynamics around the aircraft can cause the pitot static probe to read pressures slightly different from freestream introducing error into the indicated airspeed. Additionally, the pressures are read by an airspeed sensor inside the aircraft which requires the pressure to be transferred from the pitot static probe through

tubing inside the sUAS's wing. This transfer can cause slight changes in the pressures which also introduces error into the indicated airspeed reading. These errors are determined through the use of an airspeed calibration flight test.

There are multiple flight paths which can be used during these tests, but this project will use an out and back flight path due to its simplicity. This out and back course will be flown between two known points, and the distance between these two points will be measured. Averaging the time it takes the sUAS to complete the out leg and the back leg to account for the wind speed and direction, the true airspeed (TAS) of the sUAS is determined by dividing the distance by the time. The TAS can then be equated to equivalent airspeed (EAS) by correcting for the actual density at flight altitude. This is done by multiplying the TAS by the ratio of air density at altitude to the air density at standard sea level. The last step is to convert to calibrated airspeed (CAS); however, this is typically considered equal to EAS which was the case for this testing.

In order to examine the longitudinal dynamic motion of the aircraft, a flight test examining the phugoid (or long period) mode was performed. The flight test allowed the aircraft to oscillate naturally about the pitch axis by artificially exciting the phugoid mode. This excitation was provided by an abrupt step input to the elevator control in order to simulate a disturbance from trim conditions. The oscillations were then recorded by the flight data recorder for further analysis. The experimental data was then compared to the theoretical data developed in xflr5 and MATLAB. The theoretical data was developed using the rigid body equations of longitudinal motion shown in equations 1.3, 1.4, and 1.5.

$$\frac{d\alpha}{dt} = \frac{d\theta}{dt} - \frac{2g}{\overline{V}^2} V - \frac{g}{\overline{V} C_L} C_{L_\alpha} \alpha \quad [1.3]$$

$$\frac{dV}{dt} = -g(\theta - \alpha) - \frac{g}{C_L} C_{D_\alpha} \alpha - \frac{2gC_D}{\overline{V} C_L} V \quad [1.4]$$

$$\frac{d^2\theta}{dt^2} = \frac{\overline{V}^2 \rho S \bar{c}}{2I} \left(C_{m_\alpha} \alpha + C_{M_q} \frac{d\theta}{dt} \frac{\bar{c}}{\overline{V}} \right) \quad [1.5]$$

The theoretical data used the MOI determined by the bifilar pendulum along with the stability derivatives determined from the xflr5 model. This allowed for the comparison of the bifilar pendulum MOI and the MOI seen by the aircraft in flight. An examination of the effect of MOI accuracy on the theoretical dynamic motion was also performed. This involved changing the MOI by 10% and observing the difference in the predicted dynamic motion.

Chapter 2: Experimental Methods

2.1 Bifilar Pendulum Apparatus

Based on the design outlined in Jardin and Mueller, a bifilar pendulum (shown in figure 2.1) was constructed out of MDF board and paracord. The pendulum was then mounted to the ceiling using pulleys which allowed for height (h) optimization. Later, a second pendulum was constructed in an attempt to mitigate errors in the first pendulum setup as well as provide additional mounting options for future test objects (shown in figure 3.3).

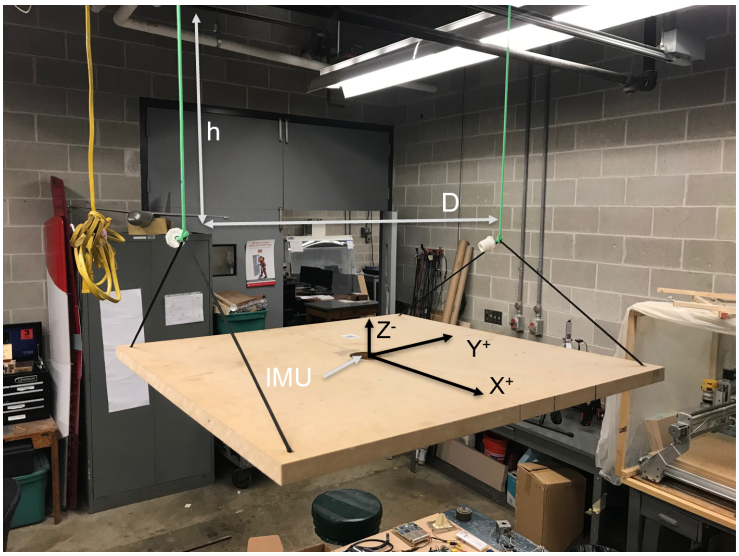

Figure 2.1: Bifilar Pendulum Original Setup

2.2 Bifilar Pendulum Setup

To set up the pendulum testing, the test object would be mounted to the pendulum with the object's center of gravity (CG) aligned with the z-axis of the pendulum to ensure the system rotated about the overall CG. The test object was also mounted such that there was no relative motion between the pendulum and the object, which often required the use of anchor ropes of

negligible mass (green anchor ropes can be seen in figure 3.9). Next, the door to the lab was closed, the air conditioning and the vent fan were turned off, and movement in the room was limited to the pendulum operator in order to ensure that no stray air currents affected the testing. Once the system and environment was ready for testing, the Inertial Measurement Unit (IMU) was placed on top of the system and switched on. The IMU contained three gyroscopic sensors (one for each primary axis of the IMU) which allowed for direct measurement of the angular velocity. It is important to note that the placement of the IMU does not affect the accuracy of the data due to the fact that the IMU is measuring angular velocity which is constant along the radius. The entire system was then rotated to the predetermined initial displacement angle of 25-35 degrees (based on the optimum found during the error analysis), held for a five-second pause to allow the system to settle, then released to freely oscillate. This process was repeated a minimum of three times for all results in order to obtain a more accurate average MOI from the multiple tests.

2.3 Bifilar Pendulum Data Processing

A MATLAB script was written to compare the experimental results to the predicted model results with varied MOI and damping coefficients. First, the experimental angular velocity data from the bifilar pendulum test along with the fixed state parameters (D, h, m, and g) were imported to MATLAB. The displacement (D) was measured using a ruler before each test, the height (h) was determined from pre-marked 1-foot intervals on the vertical pendulum strings. Finally, the mass of the test object was measured using a lab scale and added to the measured mass of the bifilar pendulum and IMU in order to determine the total mass of the system (m).

The raw input data from the IMU is shown in figure 2.2. The angular velocity data was clipped to remove the pre-test and post-test motion, and then integrated to obtain angular displacement which helped to filter out sensor noise. The resulting data is shown in figure 2.3.

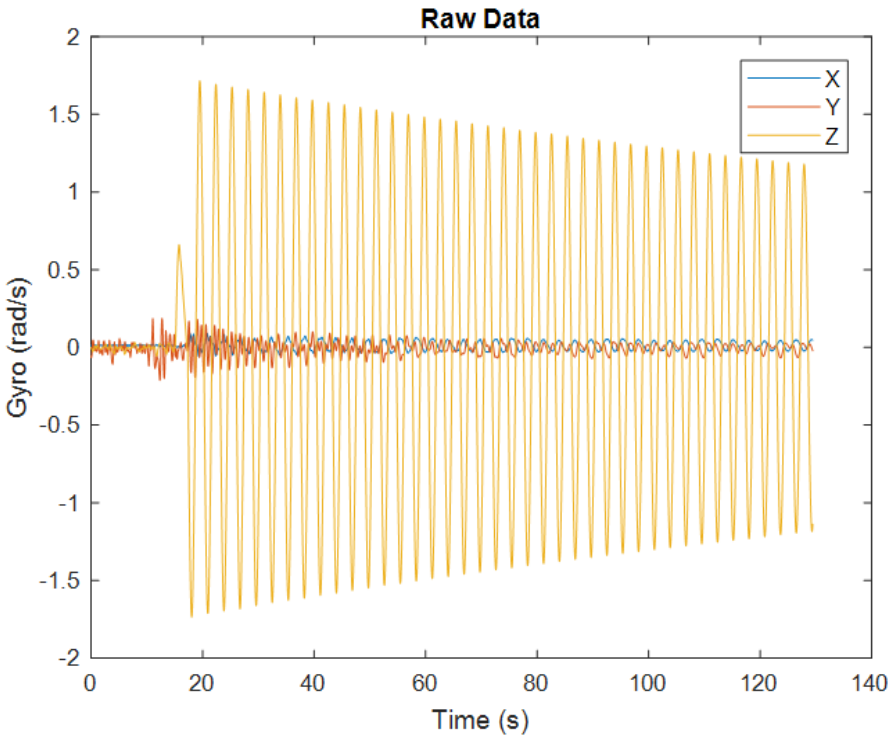

Figure 2.2: Raw Oscillation Data

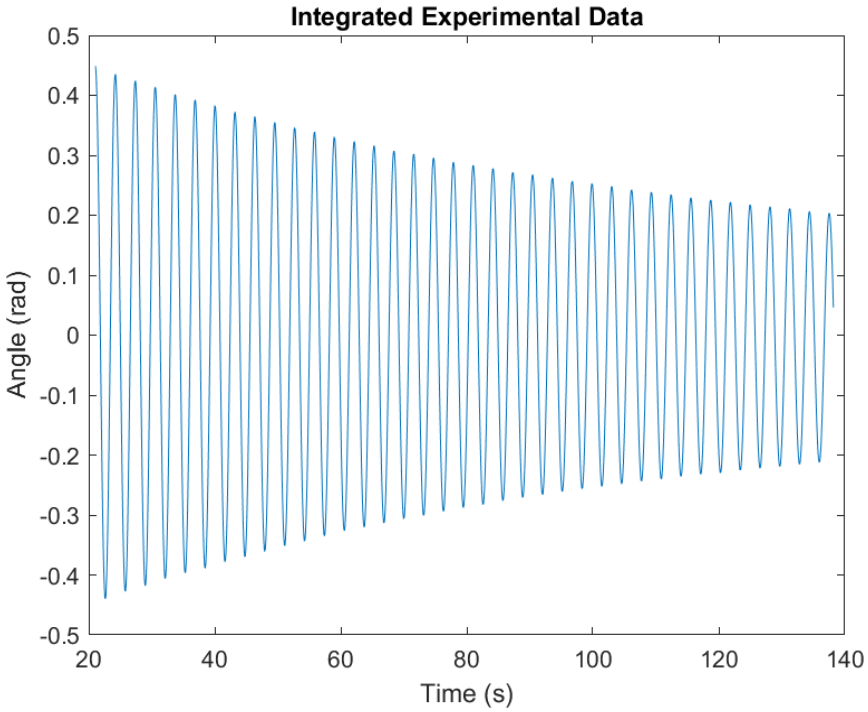

Figure 2.3: Isolated and Integrated Z-axis Oscillation Data

An Ode45 function programmed with equation 1.1 was used to simulate the bifilar pendulum motion with a constrained optimization function (fmincon) providing the changing MOI and damping coefficients. The fmincon function then finds the minimum error between the simulated results and the experimental data in order to determine the system's MOI and damping coefficients. Finally, the displacement angle (θ) versus time was plotted for both the experimental data and the model data in order to confirm the accuracy of the optimization (shown in figure 2.4).

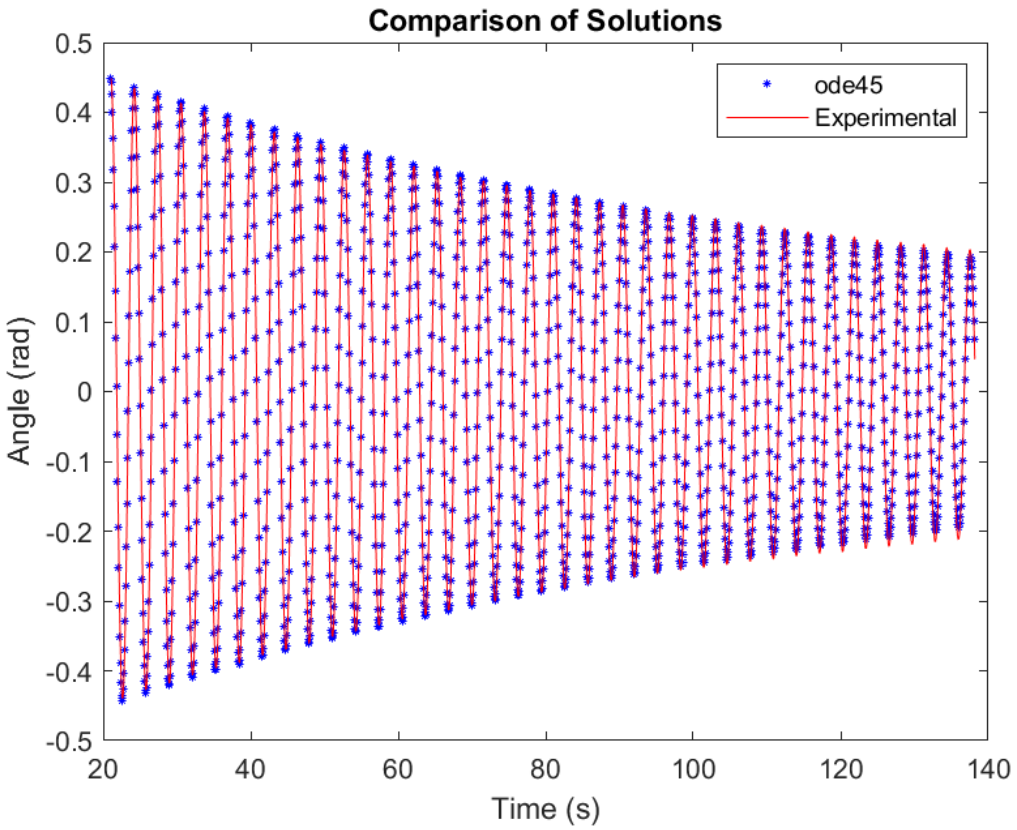

Figure 2.4: Comparison of Angular Displacement from Experimental and Computational Results

2.4 Bifilar Pendulum Accuracy Testing

In order to test the accuracy of the MOI measurements, simply shaped objects which one can analytically calculate the MOI about each axis (using simple textbook formulas) were used to compare results. SOLIDWORKS models of the test objects were also created in order to obtain the MOI from a third source for comparison. The only limitation of the analytical and SOLIDWORKS MOI calculations is their reliance on objects of uniform size and density. The test objects were not perfectly uniform, so an average size and density were used in the calculations.

The test objects chosen were the pendulum board from the original setup and a large pine beam. These objects were chosen based on the extremes of their respective inertias (the pendulum board having a small inertia (~0.3 $Kg*m^2$) and the pine beam having a much larger inertia (~3.5 $Kg*m^2$) which served as bounds for the sUAS intended for testing. Following the first round of accuracy testing, an error analysis was performed in order to determine the main sources of error and devise solutions or methods to mitigate those errors. Once the error analysis was finished, a second round of accuracy testing was performed utilizing the updated procedure and model.

2.5 Test sUAS

The sUAS that was used in the flight tests was the Mentor-G V1 which was the same sUAS used in the bifilar pendulum testing. The Mentor-G V1 is a gas-powered high-wing RC aircraft which is intended for use as a trainer aircraft for beginner RC pilots. This made it an ideal aircraft for the following flight tests due to its low speeds and slow dynamic responses. Images of the aircraft during MOI testing can be seen in figures 3.9, 3.10, and 3.11.

The aircraft was equipped with an onboard autopilot controller (the Pixhawk 1) which functions as both an autopilot and a flight data recorder. For this research project, the aircraft was flown manually by FAA-certified sUAS pilot Dr. Matthew McCrink, and the Pixhawk was used solely as a flight data recorder. The Pixhawk then recorded the key data, including the sUAS's airspeed, altitude, heading, flight path angle (θ), and attitude all as functions of time. Additionally, all flight tests were flown at Darby Dan Airport which included a 6,000 ft paved runway and ample airspace for both flight tests.

2.6 Airspeed Calibration

The airspeed calibration test used an average ground speed over an out-and-back course to determine the TAS of the Mentor-G V1 which was then converted to CAS. This out-and-back course was flown at four distinct throttle settings in order to capture the variation over the range of the aircraft's flight envelope. The calibrated airspeeds were then compared to the reported indicated airspeeds to determine the relationship between them. The flight test card used during the flight test can be found in appendix A.

2.7 Phugoid Mode Analysis

The phugoid mode flight test used a step input to the aircraft's elevator in order to excite the longitudinal dynamic modes of the Mentor-G V1. The sUAS was first trimmed in steady level unaccelerated flight at ¼ throttle. From this trim position, the pilot provided the sUAS's elevator with a step input in order to simulate a large disturbance from trim. The elevator was then returned to trim position and the sUAS was allowed to naturally oscillate. This process was repeated at ½ throttle and ¾ throttle in order to obtain a more accurate representation of the aircraft's dynamics. The flight test card used during the flight test can be found in appendix A.

After obtaining the flight test data, the oscillatory motion about the pitch aircraft was plotted in MATLAB in order to compare the experimental data to the theoretical data obtained from the rigid body equations of motion.

Chapter 3: Results

3.1 Preliminary Bifilar Pendulum Accuracy Results

To begin the inertia testing, the MOI about the z-axis for the bifilar pendulum setup was determined through analytical calculations, a SOLIDWORKS model, and experimental analysis. The MOI from each of these processes was then compared to determine the baseline accuracy of the setup.

Table 3.1: Preliminary Accuracy Test Results

Test Object	Analytical MOI [Kg*m^2]	Solidworks MOI [Kg*m^2]	Experimental MOI [Kg*m^2]
Pendulum Board	0.30829	0.30742	0.33152
Pine Beam	3.46739	3.45877	3.71667

As seen in table 3.1, the analytical and SOLIDWORKS MOI are very similar in value. The differences in the MOI can be attributed to the different calculation techniques used in each. The experimental results were similar in magnitude, but slightly higher than the two other measurements for both test objects. Using the analytical MOI as the true value, the experimental MOI had a 7.53% error for the bifilar pendulum and a 7.19% error for the pine beam. These results established the baseline accuracy for the system and a comparison for improvement of the experimental setup and procedure.

3.2 Bifilar Pendulum Parameter Optimization

Due to the extensive examination of the optimal wire separation distance (D) by Jardin and Mueller, along with the difficulty in varying the separation distance, the distance was held at 0.57 meters based on the optimum found by Jardin and Mueller. The height and initial displacement angle were varied independently in order to determine the optimum values for each parameter.

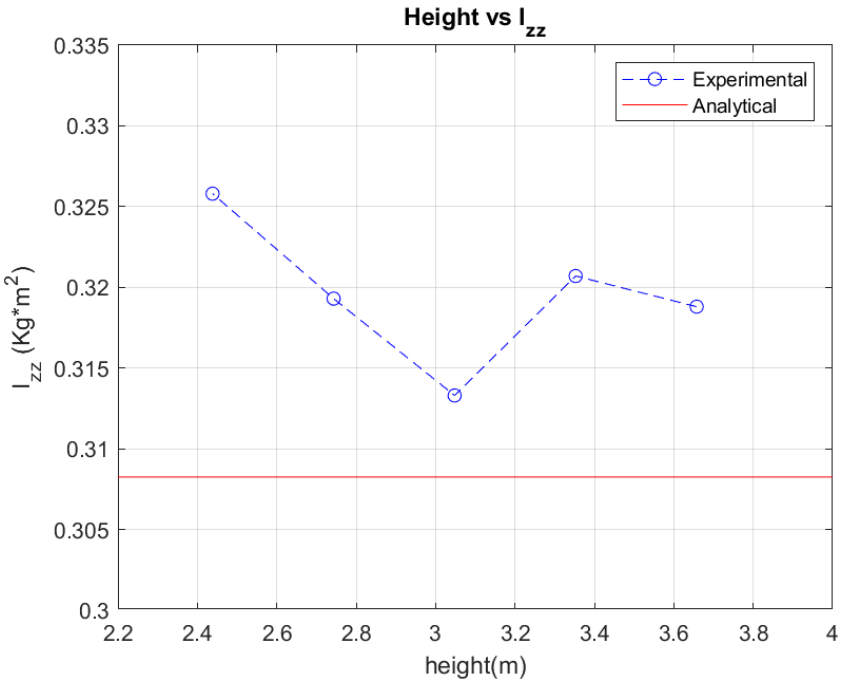

Figure 3.1: Effect of Pendulum Height on Accuracy of MOI

Figure 3.1 shows the results of the height variation testing. The red line shows the analytical MOI about the z-axis for the pendulum board. The range of heights was determined based on the environmental limitations and accessibility of the pendulum. Each data marker was determined based on an average of three tests. As can be seen in the figure, the error trends to a minimum at a height of 3.048 meters which was the height used for all of the subsequent testing.

Initially, the displacement angle was set by the pendulum operator utilizing angle markers on the pendulum plate and a datum mark on the lab wall. This caused some human error in the displacement angle which was rectified by using the integrated experimental data to set the initial angle for the computational model. The next step was to find the initial displacement angle which allowed for the most accurate result. This was done by testing three initial displacement angles: 15 degrees, 25 degrees, and 45 degrees. The 15-degree initial displacement caused a large error in the MOI measurement due to the small oscillations of the pendulum which caused the optimization function to find an inaccurate minimum error solution.

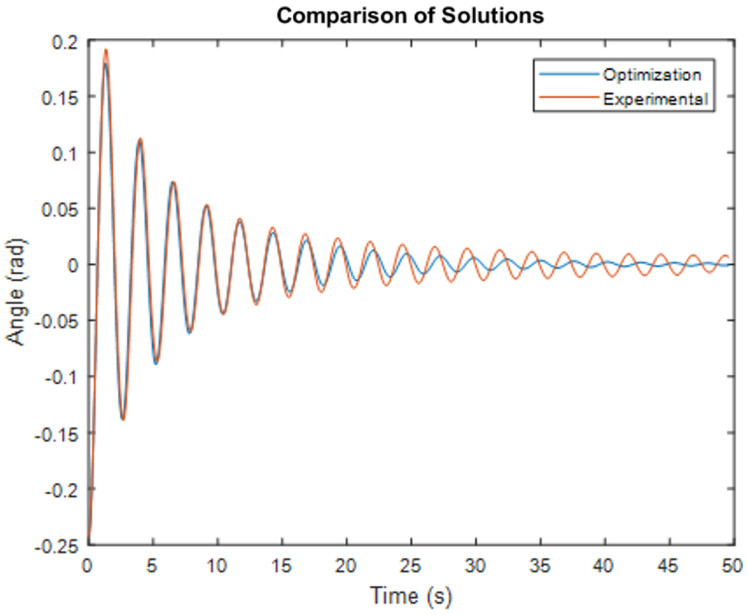

Figure 3.2: Error from Small Oscillations

As can be seen in figure 3.2, the amplitude of the experimental oscillations quickly dampens before holding at an almost constant amplitude. When attempting to match that oscillation, the Ode-45 solution over damps the system causing the fmincon function to find a minimum error

solution that does not accurately match the experimental results. This error was eliminated with both the 25- and 45-degree initial displacement; however, with the 45-degree displacement, the higher angular velocity tended to induce more translational and out of plane motion than the 25-degree initial displacement. This motion introduced new errors into the system, so the optimal initial displacement was determined to be 25 degrees. After this optimal displacement was determined, an initial displacement of 35 degrees was examined in order to determine the angle at which the oscillation became unstable. This initial displacement of 35 degrees did not exhibit the instabilities which occurred at 45 degrees and exhibited the same level of accuracy as the 25-degree displacement. From this additional investigation, it was determined that the range of acceptable initial displacement values was 25 to 35 degrees.

3.3 Bifilar Pendulum Error Analysis

The first source of error that was examined was the effect of the non-rigid support strings. As shown in figure 2.1, the pendulum board is connected to the vertical (green) strings via two black support strings which are attached to the four corners of the pendulum board. This design allowed for the board to be easily leveled before each test; however, a consequence of this design decision was the creation of an additional degree of freedom at the connection between the vertical strings and the support strings. This additional degree of freedom caused the system to violate the rigid body assumption set during the development of the non-linear equation of motion and effectively added to the height of the pendulum. An attempt was made to rectify this error using an effective height (h_e), but the difficulty of changing the support string length as well as the inconsistency of the results limited the effectiveness of this solution. Ultimately, the decision was made to adjust the design of the pendulum in order to eliminate the additional

degree of freedom. Figure 3.3 shows the modified design for the pendulum. Further testing found that both the modified setup and the original setup yielded similar levels of accuracy (accuracy results shown in table 3.2); however, the modified setup was better equipped to handle longer beam-shaped objects like the pine beam or a fixed-wing sUAS fuselage.

Figure 3.3: Modified Bifilar Pendulum Setup

3.4 Bifilar Pendulum Drag Analysis

The final step in analyzing the pendulum error was to determine the effect of drag on the moment of inertia measurement. Due to the geometry of the fixed-wing sUAS, the main wing along with the horizontal and vertical tail cause a significant increase in air resistance during rotations about each of the axes. This increase in air resistance causes an increase in moment of

inertia due to the additional mass of the air. In order to decrease this error, an empirical drag factor was determined using the foam dampers shown in figure 3.4. Foam was selected due to its low density which caused the true increase of MOI to be small compared to the pendulum's MOI. The testing utilized three sets of dampers with each set being tested in two configurations: high aspect ratio and low aspect ratio. The two orientations can be seen in figure 3.5.

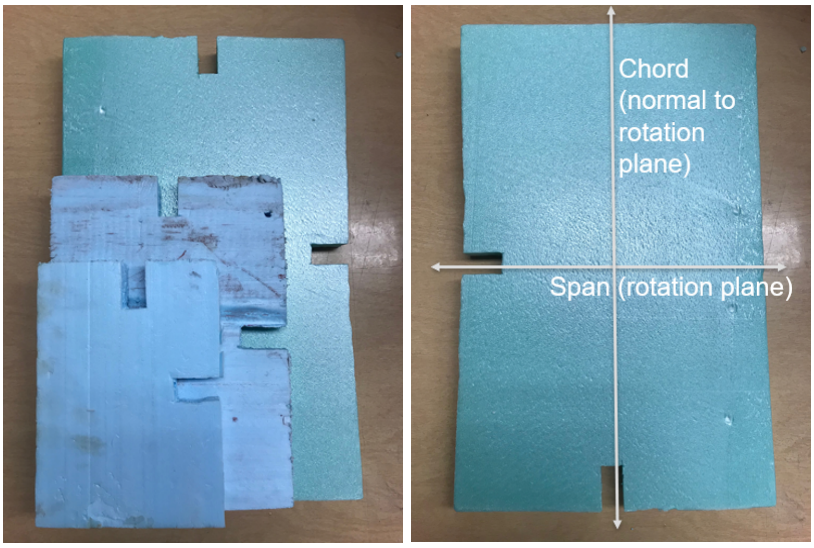

Figure 3.4: Foam Dampers

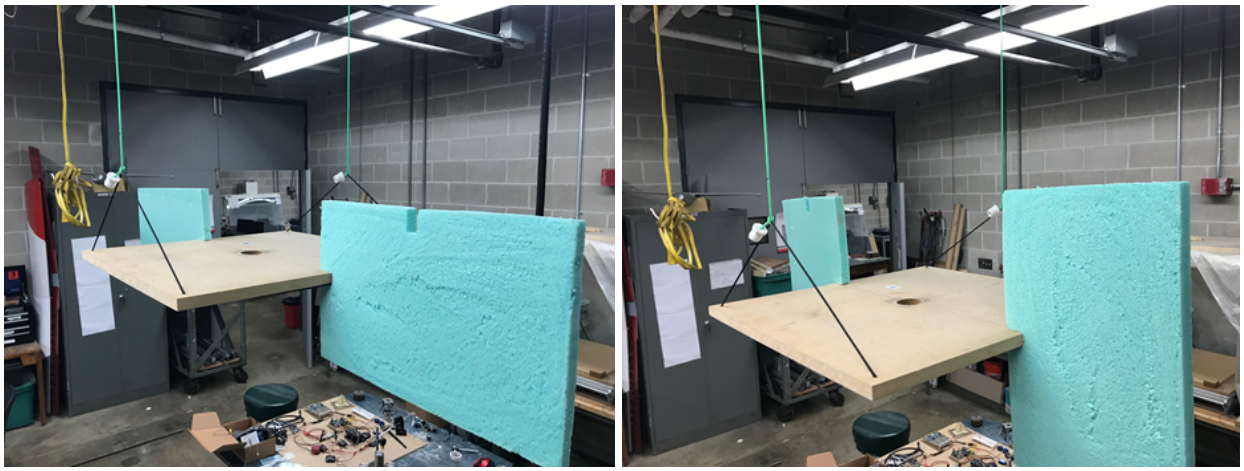

Figure 3.5: High Aspect Ratio (left) and Low Aspect Ratio (right)

The absolute error in moment of inertia for each set of dampers was plotted against the total area of both dampers as shown in figure 3.6. As can be seen in the figure, the two sets of data follow a similar trend, but have a significant difference in y-intercept. Due to this difference, the two data sets were separated into two distinct empirical drag factors based on the aspect ratio. These separated plots can be seen in figures 3.7 and 3.8 along with the corresponding empirical drag factor equations. The corresponding correction factor equation (depending on the component orientation during testing) was then used to find the correction factor for the high drag components of the sUAS.

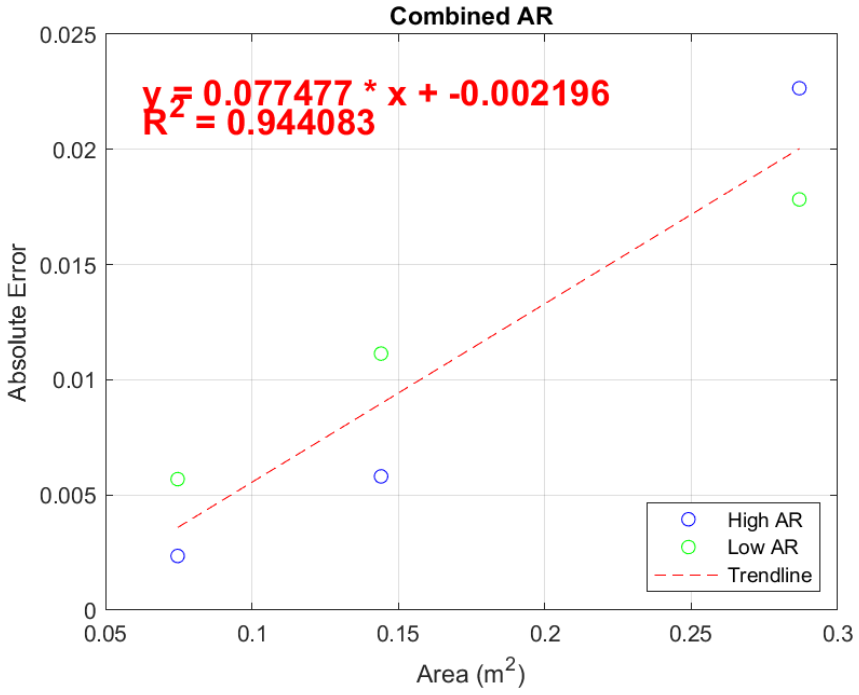

Figure 3.6: Relationship Between Damper Area and Absolute Error

3.5 Optimized Bifilar Pendulum Accuracy Results

After the procedure was optimized and the errors were mitigated, the system was again tested using the same test objects as the initial accuracy testing. The results (shown in table 3.2) were again compared to both the analytical and SOLIDWORKS calculation in order to assess the change in MOI accuracy. Since both the original bifilar pendulum setup (figure 2.1) and the modified setup (figure 3.3) were to be used in future sUAS testing, each setup was tested for accuracy. The original setup was used to test the pendulum board, and the modified setup was used to test the pine beam.

Table 3.2: Optimized Accuracy Test Results

Test Object	Analytical MOI [Kg*m^2]	Solidworks MOI [Kg*m^2]	Experimental MOI [Kg*m^2]
Pendulum Board	0.30829	0.30742	0.31110
Pine Beam	3.46739	3.45877	3.50390

Using the optimized procedure, the experimental results were much closer to the theoretical results. Using the Analytical MOI as the true value, the experimental MOI had a 0.91% error for the bifilar pendulum and a 1.05% error for the pine beam. This was a decrease of more than 6% error for both test objects.

3.6 sUAS MOI Results

After optimizing the bifilar pendulum and minimizing the residual MOI errors, the test setup was used to determine the MOI for the x, y, and z axes of the Mentor C-001. The results for the three axes are shown in table 3.3, and figures 3.9, 3.10, and 3.11 show the sUAS in the respective testing orientations.

Table 3.3: Mentor V1 MOI Results

UAV	I_{xx} [Kg*m^2]	I_{yy} [Kg*m^2]	I_{zz} [Kg*m^2]
Mentor V1	0.65583	1.25772	1.66073

3.7 Computational Flight Test Results

Utilizing the stability derivatives from xflr-5, and the moment of inertia measurement from the bifilar pendulum, the anticipated results were plotted in MATLAB using the longitudinal equations of motion. Table 3.3 shows the stability derivatives determined from the xflr-5 model.

Table 3.4: xflr-5 Stability Derivatives

Variable	Value
$C_{L\alpha}$	4.74
$C_{D\alpha}$	0.63
$C_{m\alpha}$	-0.71
C_{mq}	-10.16

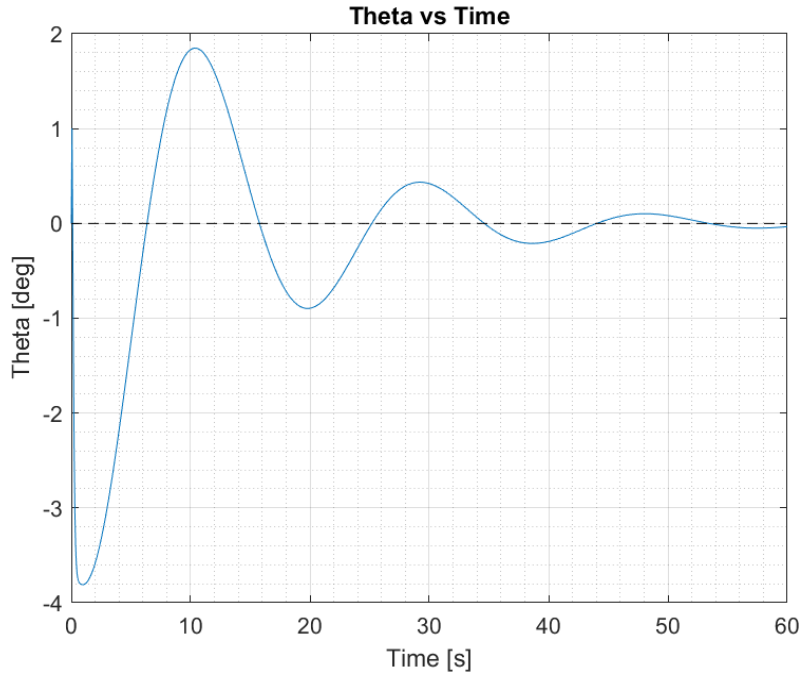

Figure 3.12: Pitch Oscillation at Nominal MOI

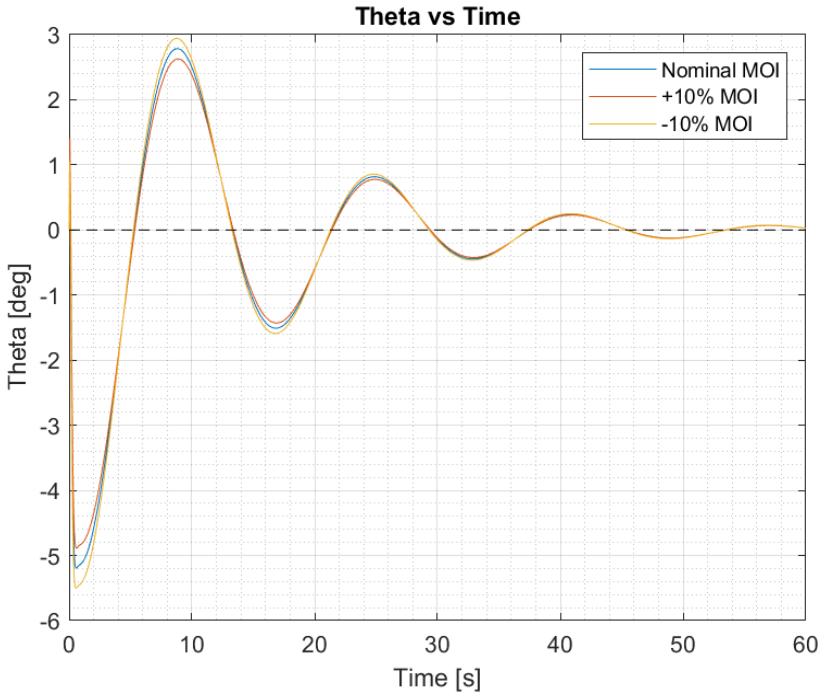

Figure 3.13: Pitch Oscillation with Varied MOI

Table 3.5: Response Change with Varied MOI

MOI	Overshoot [deg]	% Error	Natural Freq. [rad/s]	% Error	Damping Ratio	% Error
1.257 (nom.)	5.19	-	0.389	-	0.192	-
1.383 (+10%)	4.89	5.78	0.395	1.49	0.191	0.52
1.131 (-10%)	5.48	5.59	0.393	1.51	0.193	0.52

In order to obtain the results shown in figure 3.12, the sUAS (set at a steady state velocity of 21.4 m/s) was provided an initial angular velocity of 1 deg/s to simulate the planned rudder deflection of the flight test. The sUAS was then allowed to oscillate freely according to the longitudinal equations of motion.

In order to determine the effect of an inaccurate MOI measurement, figure 3.13 shows a comparison of the resulting oscillation with varied MOI. Table 3.4 also shows a summary of the response changes with change in MOI. As can be seen in figure 3.13, a change of +/- 10% in the MOI does not have a significant impact on the resulting motion of the sUAS. The responses vary slightly at the beginning of the oscillation, but merge together as time moves forward. Table 3.4 shows similar results with the natural frequency and damping ratio remaining relatively unchanged (~1% error). The +/-10% change in MOI does have a more adverse effect on the overshoot (~5% error); however, the overshoot is a less impactful response characteristic. While this is the case for the longitudinal dynamics of the sUAS, the accuracy of the MOI may be more important for the lateral or directional dynamics of the sUAS.

The behavior of the dynamic response was greatly affected by changes in the stability derivative values (particularly the drag related derivatives). Since xflr-5 stability models do not include the fuselage, the additional drag effect of the fuselage must be estimated through the use of

simplified equations. While this method can provide a rough estimate of the drag effects, it cannot account for the complex flow characteristics the aircraft will see in flight. In order to obtain better computational data for comparison to the flight test data, a more accurate solution for determining the aircraft's stability derivatives may be required.

3.8 Flight Test Results

Due to changes in Ohio State University policy after the outbreak of COVID-19, the planned flight tests could not be completed. Due to the importance of validating the bifilar pendulum measurements through flight testing, completion of the planned flight tests will be the first step to completing future work on the project.

Chapter 4: Conclusions and Future Work

4.1 MOI Testing Conclusions

After the completion of the bifilar pendulum testing, the results show the bifilar pendulum is capable of providing accurate MOI measurements while keeping cost and complexity low. From the optimized accuracy test results, the bifilar pendulum was capable of obtaining MOI measurements for both high inertia and low inertia objects within 1% accuracy. The bifilar pendulum was also adaptable to multiple configurations making it ideal for a wide variety of sUAS platforms.

4.2 Future MOI Testing

Due to the nature of an undergraduate research thesis, the scope of this project had to be limited in order to meet the required graduation deadline. Because of this limitation, there was not as much time to fully investigate all of the errors in the bifilar pendulum. When considering the measurements of fixed-wing aircraft, one of the most important errors is the effect of drag on the moment of inertia. While this error was corrected using an experimentally determined empirical drag factor, the mitigation of this error would benefit from a more detailed analysis. Specifically, an examination into the effects of length from the center of rotation (at pendulum CG) to the center of pressure for both symmetric and asymmetric drag-inducing bodies. In this research project, the empirical drag factor was assumed to be independent of the lever arm length; however, this was not confirmed through experimental analysis. Additionally, the foam dampers were tested in a symmetric configuration in order to keep the bifilar pendulum level. Some of the drag-inducing bodies on the aircraft (such as the vertical and horizontal tail), are in an

asymmetric orientation during the moment of inertia measurements which could affect the drag factor.

While this research project only examined the moments of inertia about the primary axes (I_{xx}, I_{yy}, and I_{zz}), the coupling of these axes (I_{xy}, I_{xz}, and I_{zy}) are equally important in determining the dynamic motion of a sUAS. The bifilar pendulum could be used to examine these moments of inertia as well in order to fully capture the sUAS's dynamic motion. Additionally, the primary axes were assumed to be inline with the body axes of the sUAS. It is unlikely that the degree of rotation between the two frames is significant; however, it would be useful to determine the offset in order to more accurately capture the sUAS's primary moments of inertia.

4.3 Flight Test Conclusions

Without the flight test data, the MOI measurements from the bifilar pendulum could not be validated. The variation of the longitudinal MOI (I_{yy}) within the simulated longitudinal motion showed that the accuracy of the MOI measurement did not have a significant effect on the predicted motion of the aircraft. Further analysis would be required in order to determine the importance of MOI accuracy for the lateral and directional dynamics of the UAV.

4.4 Future Flight Testing

Due to the limited flight availability and poor weather conditions along with the increased difficulty in performing lateral and directional dynamic flight tests, the flight tests were limited to examining the longitudinal dynamics. However, validating the lateral and directional dynamics from the bifilar pendulum would be the next step in assessing the overall accuracy of

the moments of inertia measurements. Additionally, utilizing flight tests to validate the future non-primary axis MOI measurements from the bifilar pendulum.

Another area of improvement would be to use the autopilot capabilities of the Pixhawk to automate the flight tests. This would allow for the removal of pilot errors during the test flights which may cause errors in the oscillation data, and would help to streamline the flight testing process.

UAV Flight Test Card

Flight Test Plan

The calibration test will use an average ground speed over an out and back course to determine the TAS of the Mentor C-002 which will then be converted to CAS. This out and back course will be flown at four distinct IAS in order to capture the variation over the range of the aircraft's flight envelope. The calibrated airspeeds will then be compared to the flight test indicated airspeeds to determine the relationship between them.

Flight Profile (top-view)

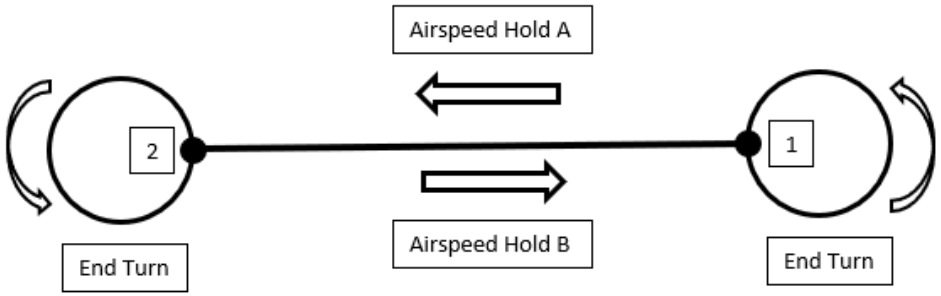

Fight Test: Airspeed Calibration

UAV Pilot: Dr. M. McCrink

Flight Test Card:

Flight Leg	Flight Maneuver Procedure
Airspeed Hold A	SLUF at ¼ throttle from point 1 to point 2
Airspeed Hold B	SLUF at ¼ throttle from point 2 to point 1
End Turn	At pilot's discretion to line up for airspeed hold flight legs
Repeat Test	Repeat all legs at same throttle setting
Next Test	Repeat flight test at throttle settings of ½ and ¾

Source: AAE 5612 Aircraft Performance and Flight Testing Engineering, Dr. Whitfield

Flight Test Plan

The phugoid mode flight test will use a step input to the aircraft's elevator in order to excite the longitudinal dynamic modes of the Mentor C-002. The aircraft will first be trimmed in steady level unaccelerated flight at ¼ throttle. From this trim position, the pilot will provide the aircraft's elevator with a step input in order to simulate a large disturbance from trim. The elevator will then be returned to trim position and the aircraft will be allowed to naturally oscillate. This process will be repeated at ½ throttle and ¾ throttle in order obtain a more accurate representation of the aircraft's dynamics.

Flight Profile (top-view)

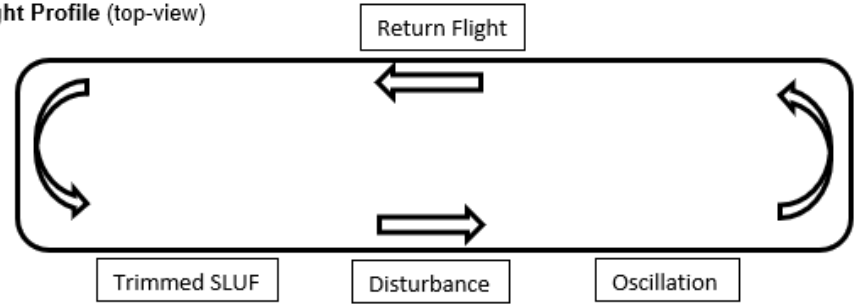

Flight Profile (side-view of disturbance and oscillation leg)

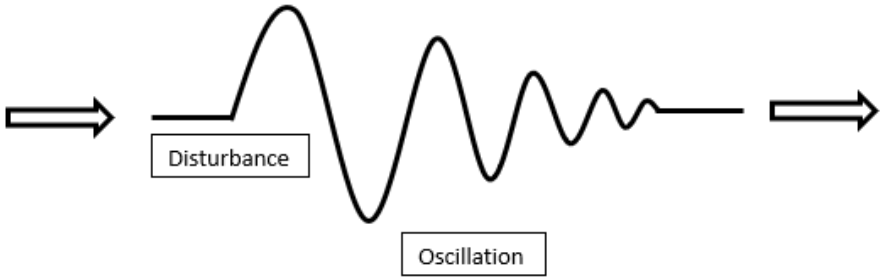

Fight Test: Phugoid Mode

UAV Pilot: Dr. M. McCrink

Flight Test Card:

Flight Leg	Flight Maneuver Procedure
Trimmed SLUF	Establish constant speed trimmed straight and level flight, ¼ throttle
Disturbance	Provide step input to elevator
Oscillation	Return elevator to trim position and allow aircraft to oscillate without pilot input
Return Flight	At pilot's discretion to align for trimmed SLUF
Repeat	Repeat trimmed flight, disturbance, and oscillation at same throttle setting
Changing throttle setting	Repeat flight test with throttle settings of ½ and ¾

Source: AAE 5612 Aircraft Performance and Flight Testing Engineering, Dr. Whitfield

Figures

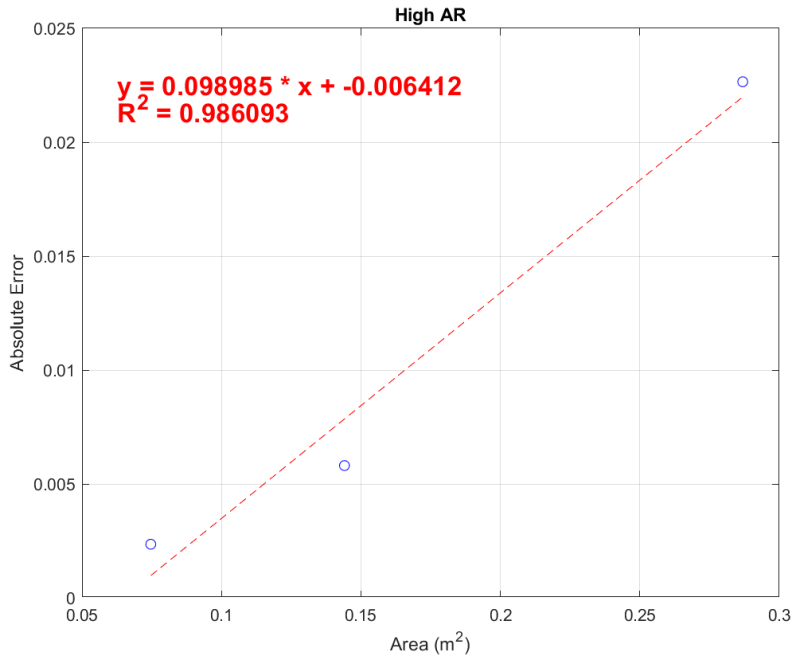

Figure 3.7: Relationship Between Damper Area and Absolute Error (High AR Only)

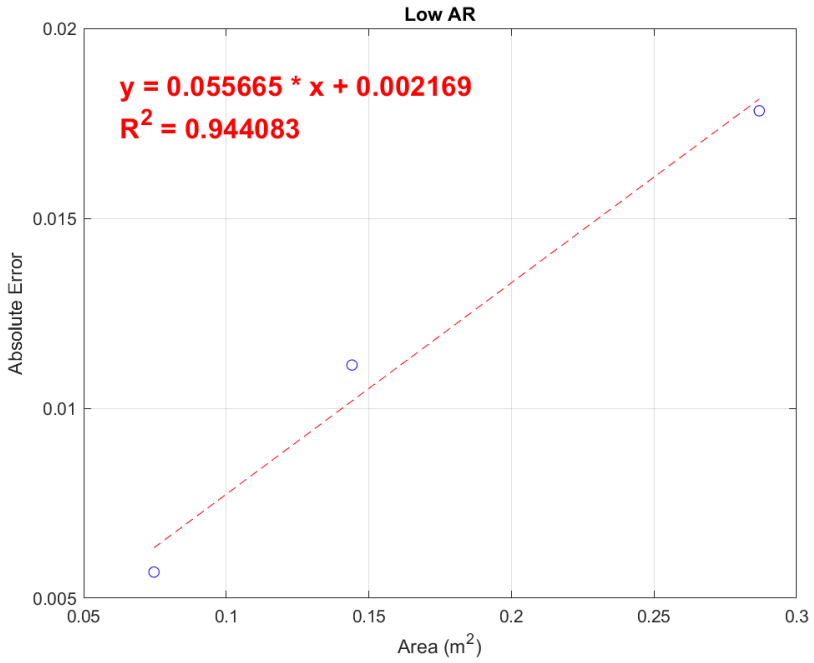

Figure 3.8: Relationship Between Damper Area and Absolute Error (Low AR Only)

Figure 3.9: Mentor V1 in I_{yy} Testing Configuration

Figure 3.10: Mentor V1 in I_{xx} Testing Configuration

Figure 3.11: Mentor V1 in I_{zz} Testing Configuration

References

[1] Chin, A. W., Herrera, C. W., Spivey, N. W., Fladung, W. W., and Cloutier, D. W., "Experimental Validation of the Dynamic Inertia Measurement Method to find the Mass Properties of an Iron Bird Test Article," *56th AIAA/ASCE/AHS/ASC Structures, Structural Dynamics, and Materials Conference*, Feb. 2015, pp. 4–11.

[2] Boucher R, Rich D, Crane H, Matheny, C. "A Method for Measuring the Product of Inertia and the Inclination of the Principal Longitudinal Axis of Inertia of An Airplane". *NACA TN 3084.* 1954, pp. 5-16.

[3] Barnes C, Woodfield A. "Measurement of the Moments and Product of Inertia of the Fairey Delta 2 Aircraft." *Aeronautical Research Council, Reports and Memoranda No. 3620.* 1970, pp. 3-15.

[4] Gallagher G, Higgins L, Khinoo L, Pierce P. "Fixed Wing Performance." *US Naval Test Pilot School Test Manual. USNTPS-FTM-NO. 108.* 1992, pp. 1.1-1.17

[5] "Flight Test Guide For Certification Of Transport Category Airplanes." *U.S. Department of Transportation Federal Aviation Administration. AC No: 25-7C.* 2012, pp. 9-1-9-5

[6] Jardin, M., and Mueller, E., "Optimized Measurements of UAV Mass Moment of Inertia with a Bifilar Pendulum," *AIAA Guidance, Navigation and Control Conference and Exhibit*, 2007, pp. 1–22.

[7] Landman, D., Britcher, C., and Bennett, W., "A power-on full-scale wind tunnel test of a UAV," *17th Applied Aerodynamics Conference*, 1999, pp. 5–22.

[8] Michalowski, B., and Varano, N., "UAV flight test characterization using minimal test equipment," *2017 International Conference on Unmanned Aircraft Systems (ICUAS)*, 2017, pp. 1–5.

[9] Castillo, O. G., and Londner, E., "UAV Flight Testing with an Airborne Sonic Anemometer, IMU and GPS," *28th AIAA Applied Aerodynamics Conference*, 2010, pp. 3–10.

[10] Phillips, W. F., and Phillips, W. F., *Mechanics of flight*, Hoboken, NJ: John Wiley & Sons, Inc., 2010, pp. 813–878.

[11] i3dthemes.com. Stability and Control, code7700.com/aero_stability_and_control.htm.

[12] Whitfield, Clifford. "AAE 5612: Airspeed Calibration" Flight Test Engineering, 15 Jan. 2020, The Ohio State University. Microsoft PowerPoint presentation.

[13] Whitfield, Clifford. "AAE 5612: Longitudinal Stability" Flight Test Engineering, 15 Jan. 2020, The Ohio State University. Microsoft PowerPoint presentation.